Asian Journal of Chemistry; Vol. 37, No. 2 (2025), 503-510

ASIAN JOURNAL OF CHEMISTRY

https://doi.org/10.14233/ajchem.2025.33322

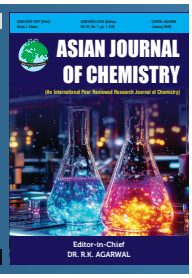

Synthesis, Characterization and Magnetic Properties of $SmFe_xO_3$ and $LaFe_xO_3$ Perovskites with Iron Excess and Deficiency (x = 1.05, 0.95)

K. RAMMOHAN[1,2], G. VIJAYA LAKSHMI[1,3,*] and G. RAMESH[4]

[1]Department of Chemistry, University College of Science, Osmania University, Hyderabad-500007, India
[2]Department of M.Sc. 5 Year Integrated Chemistry, University P.G. College, Palamuru University, Mahbubnagar-509001, India
[3]Department of Chemistry, Veeranari Chakali Ilamma Women's University, Koti, Hyderabad-500095, India
[4]Department of Chemistry, Vardhaman College of Engineering, Hyderabad-501218, India

*Corresponding author: E-mail: gvjlakshmi@gmail.com

Received: 25 December 2024; *Accepted*: 29 January 2025; *Published online*: 31 January 2025; AJC-21904

$SmFeO_3$ (SFO) and $LaFeO_3$ (LFO) perovskites with excess and deficient iron ($SmFe_{1.05}O_3$, $SmFe_{0.95}O_3$ and $LaFe_{1.05}O_3$, $LaFe_{0.95}O_3$) were synthesized using the sol-gel method, achieving a quantitative yield of 98%. The materials were thoroughly characterized using powder X-ray diffraction (p-XRD), field emission scanning electron microscopy with energy-dispersive X-ray spectroscopy (FESEM-EDS), UV-visible diffuse reflectance spectroscopy (UV-Vis DRS), X-ray photoelectron spectroscopy (XPS), and vibrating sample magnetometry (VSM) analysis. The p-XRD confirmed the successful synthesis of the iron-modified SFO and LFO perovskites with an orthorhombic structure, crystallizing in the P_{nma} space group and the La^{3+} forms an eight-coordinate geometry with O^{2-} atoms in the perovskite lattice. The orthorhombic structure and phase purity, irregular morphology conformed by p-XRD and FESEM analysis. The elemental composition and the surface architecture and chemical valence state of key elements of above perovskites by EDS and XPS analysis. The band gap energies of $SmFe_{1.05}O_3$ (1.96 eV) $SmFe_{0.95}O_3$ (2.04 eV) and $LaFe_{1.05}O_3$ (2.00 eV) $LaFe_{0.95}O_3$ (2.11 eV) were determined using UV-Vis diffuse reflectance spectroscopy (UV-Vis DRS). VSM analysis revealed that iron-deficient $LaFe_xO_3$ ($LaFe_{0.95}O_3$) exhibited paramagnetic behaviour with higher saturation magnetization, while iron-excess $SmFe_xO_3$ ($SmFe_{1.05}O_3$) also displayed paramagnetic behaviour.

Keywords: Perovskites, Iron excess, Iron deficiency, VSM analysis, Magnetic properties, Paramagnetism.

INTRODUCTION

L. Perovski had discovered a cubic crystal structure with the chemical composition $CaTiO_3$ [1,2]. In perovskite crystals, cation A is located between the BO_6 octahedron connected through the apex angle, while cation B possessing six-fold coordination is surrounded by an octahedron of anions [3,4]. Owing to their physical, chemical and multifunctional properties, they display significant chemical and physical characteristics, including optoelectricity, half-metallicity, a high absorption coefficient, long-range ambipolar charge transport, a high diel-ectric constant, excitation-binding energy and ferroelectricity [5-7].

In 21st century, the perovskites have seen a sharp increase in interest in recent years as they find extensive use in electrical conductors, solid oxide fuel cells, magnetic devices and catalysis [8]. In addition to being electrical conductors, perovskites are paramagnetic, photocatalytic, thermoelectric and dielectric materials with exceptional thermal and chemical durability. Iron in the B-site, the "catalytic" location of the perovskite structure, guarantees significant reactivity to oxygen and oxygenated molecules [9-12].

Iron excess and deficiency in $SmFeO_3$ and $LaFeO_3$ perovskites were prepared using the sol-gel method characterized by using powder XRD, FESEM-EDS, UV-visible diffuse reflectance, X-ray photoelectron spectroscopy and VSM. The results presented here indicate the possibility of synthesizing fine perovskites with quantitative yield (98%) *via* the sol-gel method. The results confirmed the successful synthesis of above perovskites with an orthorhombic structure, crystallizing in the orthorhombic P_{nma} space group [13,14]. La^{3+} is coordinated to eight O_2 atoms in a way that has eight-coordinates. The current work is an attempt in this direction and designed at preparing the iron based perovskites. This synthesized perovskites materials

exhibited paramagnetic with higher saturation magnetization and absorb more visible light in the photodegradation. Hence, this perovskites act also as photocatalyst in the photodegradation process. This study provides insights into the influence of iron stoichiometry on the magnetic and structural properties of SFO and LFO perovskites, synthesized *via* an efficient sol-gel method.

EXPERIMENTAL

Lanthanum(III) nitrate hexahydrate [$La(NO_3)_3{\cdot}6H_2O$] and samarium(III) nitrate hexahydrate [$Sm(NO_3)_3{\cdot}6H_2O$] were procured from Sisco Research Laboratories Pvt. Ltd., India. Iron(III) nitrate nonahydrate [$(Fe(NO_3)_3{\cdot}9H_2O)$], ethyl alcohol ethylene glycol (EG, HO-C_4H_4OH), citric acid and ammonia were obtained from the Research Lab Fine Chem Industries, India. All solvents were of analytical reagent grade and used without further purification.

Characterization: The UV-visible diffuse reflectance spectra (UV-Vis DRS) were recorded using a spectrophotometer (model JASCO V650) and an integrating sphere attachment to collect the diffuse reflectance from the powder samples. Powder X-ray diffraction (p-XRD) patterns of the as-synthesized iron excess and iron deficiency of SFO and LFO perovskite materials were collected over a wide range of 2θ angles from 10º to 80º using a Rigaku MiniFlex powder diffractometer with Cu*K*α radiation (λ = 1.5406 Å). The surface morphology, microstructure of above perovskites were investigated using high-resolution CARL ZEISS SUPRA 55 field emission scanning electron microscopes. An Oxford Instruments X-MaxN EDS detector was used to acquire the spectra from specific regions of interest on the sample surface. Mapping of the constituent elements (Sm, La, Fe and O) was performed to visualize their spatial distribution and assess compositional homogeneity across the sample surface. The magnetic properties of these perovskites were characterized using a Lake Shore 8600 series VSM. The X-ray photoelectron spectroscopy (XPS) was employed to investigate the chemical states and electronic structure of the perovskite materials. The XPS measurements were performed using a Kratos ESCA 3400 spectrometer equipped with an Al Kα X-ray source (hν = 1486.6 eV).

(A) Synthesis of excess and deficiency of iron in LFO perovskites: Sol-gel and calcination methods were used to synthesize the perovskite LFO powders. In brief, $La(NO_3)_3{\cdot}6H_2O$ (5 g) and $Fe(NO_3)_3{\cdot}9H_2O$ (4.8 g and 4.4 g) in a ratio of 1:1.05 and 1:0.95 were dissolved in 200 mL of ethyl alcohol at room temperature for 2 h of constant stirring followed by the addition of citric acid (5.5 g) and again stirred for 1 h. Now, ammonia solution was added to adjust the mixture at pH 7 at 70 ºC. Then, added 3.6 mL of ethylene glycol and 3.2 mL of ethylene glycol solution to 100 mL of 50% above solution at 160 ºC. The mixture was stirred until it turned black before being ground for calcination in a muffle furnace at 800 ºC for 8 h. The result was 98% pure excess and deficiency of iron in LFO perovskite materials in powdered form.

The reactions involved in the synthesis of excess and deficiency of iron in LFO perovskite materials are as follows:

$$La(NO_3)_3{\cdot}6H_2O + xFe(NO_3)_3{\cdot}9H_2O + C_6H_8O_7{\cdot}H_2O \longrightarrow LaFe_xO_3 + 6CO_2 + 3N_2 + nH_2O$$

where x = 1.05 (excess) or 0.95 (deficiency).

(B) Synthesis of excess and deficiency of iron in SFO perovskites: The same process was followed as mentioned above using $Sm(NO_3)_3{\cdot}6H_2O$ instead of $La(NO_3)_3{\cdot}6H_2O$.The reactions involved in the synthesis of excess and deficiency of iron in SFO perovskite materials are as follows:

$$Sm(NO_3)_3{\cdot}6H_2O + xFe(NO_3)_3{\cdot}9H_2O + C_6H_8O_7{\cdot}H_2O \longrightarrow SmFe_xO_3 + 6CO_2 + 3N_2 + nH_2O$$

where x = 1.05 (excess) or 0.95 (deficiency).

RESULTS AND DISCUSSION

UV-visible spectroscopy: The UV-Vis DRS spectra of excess and deficiency of iron in SFO prepared by the sol-gel method was observed at maximum wavelengths of 662 nm and 630 nm (Fig. 1). As the species get closer to each other, they absorb more of each other. With the sol-gel method, this means that closer species are present in the excess and deficiency of iron in the SFO structures made with an open structure [15,16]. The measured maximum value shows that SFO made in this way is active as a photocatalyst in the visible wavelength range. Meanwhile, the maximum wavelengths of excess and deficiency of iron in LFO were found at 617nm and 603 nm [17] (Fig. 1). LFO structures prepared by the sol-gel approach in both cases are closer together since the absorption increases as the contents get closer [18].

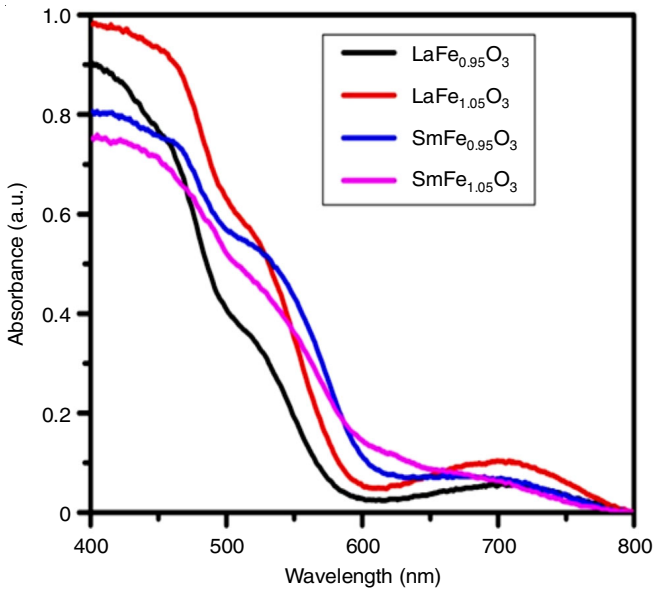

Fig. 1. UV-visible diffuse reflectance spectrum of synthesized perovskites by sol-gel method for powder samples obtained

Band gap energy: Fig. 2 shows the Kubelka-Munk (KM) plots of the synthesized perovskites. SFO pervoskites had a bandgap of 1.96 eV and 2.04 eV for excess and deficiency of iron, while LFO nanoparticles had 2.00 and 2.11 eV. These values are smaller than the bandgap energies of orthorhombic SFO and LFO perovskites [19,20] and is useful for further studies of photocatalysis.

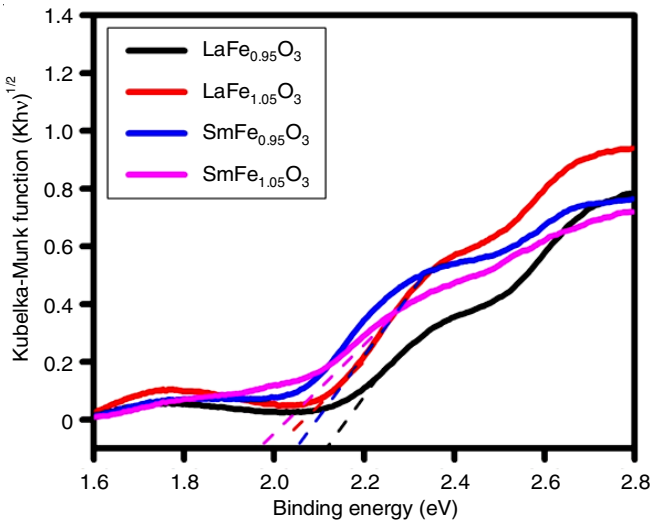

Fig. 2. KM plot band gap energy of synthesized perovskites

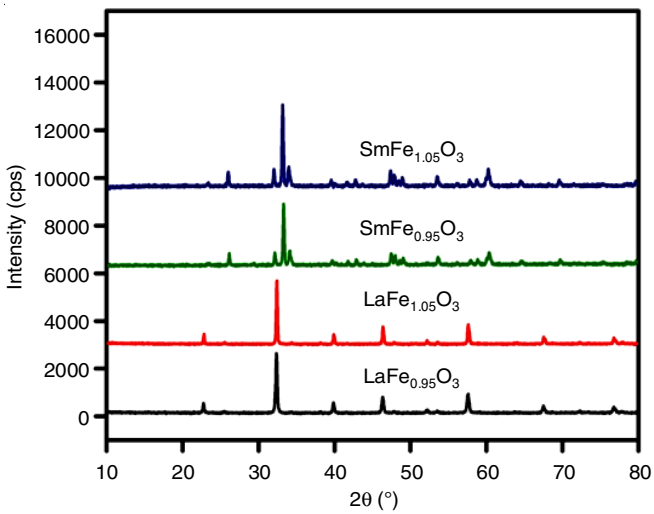

Fig. 3. X-ray diffraction pattern of synthesized perovskites powders

XRD studies: X-ray diffraction analysis confirmed that the powder was composed of synthesized perovskites with an orthorhombic structure, crystallizing in the orthorhombic P_{nma} space group by comparing the results to the standard JCPDS card nos. 86-1330, 88-0641 and 73-1345, respectively [21,22]. Importantly, no secondary phases except the perovskite structure were found to be present. The X-ray diffraction pattern was used to determine the compound's lattice parameters using the formula: $d = (h^2/a^2 + k^2/b^2 + l^2/c^2)^{-1/2}$, where (*hkl*) are indices of crystallographic planes; d is the interplanar distance and *a*,*b*,*c* are the lattice parameters [23]. The lattice constants *a*, *b* and *c* for powdered synthesised perovskites using the sol-gel method are 5.6001 Å, 7.706 Å, 5.3995 Å and 5.5647 Å, 7.8551 Å, 5.556 Å. The synthesized perovskites have unit cell volumes of 233.01 $Å^3$ and 242.86 $Å^3$. The Debye Scherrer's formula was used to determine the change in crystallite size of the prepared photocatalyst samples that were calcined at 800 ºC

$$d_{hkl} = \frac{K\lambda}{\beta_{0.5}\cos\theta}$$

where K is the particle's form factor (K = 0.94); d_{hkl} is the mean crystallite size, λ is the X-ray (Cu*K*α) wavelength, $\beta_{0.5}$ is the peak broadening at half maximum intensity, and θ is the Bragg angle for the diffraction (Fig. 3). The X-ray diffraction (XRD) patterns of synthesized perovskites show orthorhombic structure.

FESEM and EDS studies: FESEM and EDS spectra were used to examine iron deficiency and excess of SFO and LFO perovskite [24]. FESEM images of iron deficiency and excess of SFO and LFO perovskite reveal bulky and irregularly shaped lumps that stick together. The EDS analysis confirms that the chemical ratios of La, Sm, Fe and O in pure LaFeO and SmFeO are stoichiometric. The weight percentages of each element are provided in the corresponding EDS images. Figs. 4 and 5 illustrate that there is no significant change in the FESEM and EDS results for SFO and LFO perovskites with iron deficiency and excess.

XPS studies: To better understand the surface architecture and chemical valence state of key elements an X-ray photoelectron spectroscopy (XPS) study was conducted. Fig. 6 and 7 show the XPS spectra of as-synthesized iron deficiency and excess of SFO, repectively. Fig. 6a and 7a shows the XPS survey spectrum of the SFO nanostructure, which confirms the presence of the elements samarium (Sm), iron (Fe) and oxygen (O) in the sample. Meanwhile, Sm has exhibited two significant signals at 1084.63 eV and 1132.20 eV, which were ascribed as the binding energies of Sm $3d_{5/2}$ and Sm $3d_{3/2}$ (Fig. 6b and 7b). According to the high resolution XPS survey of Fe in Fig. 6c and 7c, it is present as both Fe^{2+} and Fe^{3+} oxidation states in the SFO perovskites, which shows two individual peaks with binding energies of Fe $2p_{3/2}$ and Fe $2p_{1/2}$ at 712.83eV, 727.90eV, and 745.25 eV. The strong overlap between Fe $2p_{3/2}$ and Sm $3d_{3/2}$ in this location makes it difficult to precisely calculate the Fe^{2+}/Fe^{3+} ratio. Furthermore, following Sm-Fe interactions, the Sm 3d and Fe 2p peaks shift to lower and higher binding energies, respectively, compared to the usual peak values [25]. In comparison to the normal peak values following Sm-Fe interactions, fitted binding energies had lower and higher binding energies. The oxygen (O^{2-}) in the $SmFeO_3$ perovskite lattice was detected in Fig. 6d and 7d by two peaks at 531.18 eVand 532.88 eV.

Figs. 8 and 9 contain the binding energies data of as-synthesized iron deficiency and excess of LFO perovskites, respectively. The XPS survey spectra of iron deficiency and excess of LFO perovskites is shown in Fig. 8a and 9a which confirms the co-existence of the elements lanthanum (La), iron (Fe) and oxygen (O). Meanwhile, La has exhibited two significant signals at 836.94 eV and 865.73 eV were ascribed as binding energies of La $3d_{5/2}$ and La $3d_{3/2}$, respectively (Fig. 8b and 9b) and were allocated to the fundamental spectra of La^{3+} in the oxide structure [26]. The Fe is present in both Fe^{2+} and Fe^{3+} oxidation states in the LFO perovskites, according to the high resolution XPS survey of Fe in Fig. 8c and 9c, which shows two individual peaks with binding energies of Fe $2p_{3/2}$ and Fe $2p_{1/2}$ at 710.86 eV, 724.70 eVand 743.65 eV. The strong overlap between Fe $2p_{3/2}$ and La $3d_{3/2}$ in this location makes it hard to precisely determine the Fe^{2+}/Fe^{3+} ratio. In addition, following La-Fe interactions, the La 3d and Fe 2p peaks are moved lower and higher

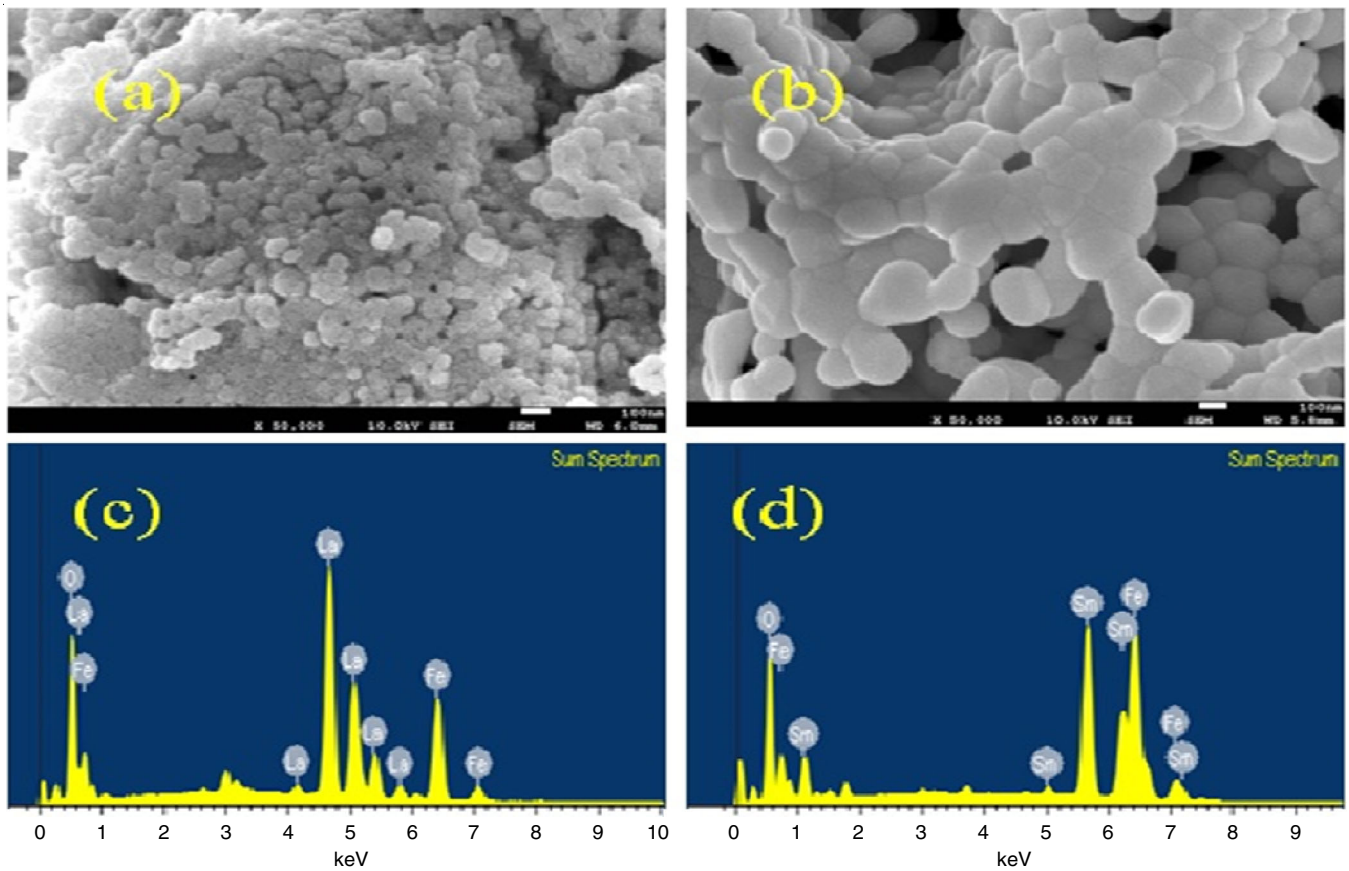

Fig. 4. (a,b) FESEM of iron deficiency of LFO and SFO and (c,d) EDS of iron deficiency of LFO and SFO

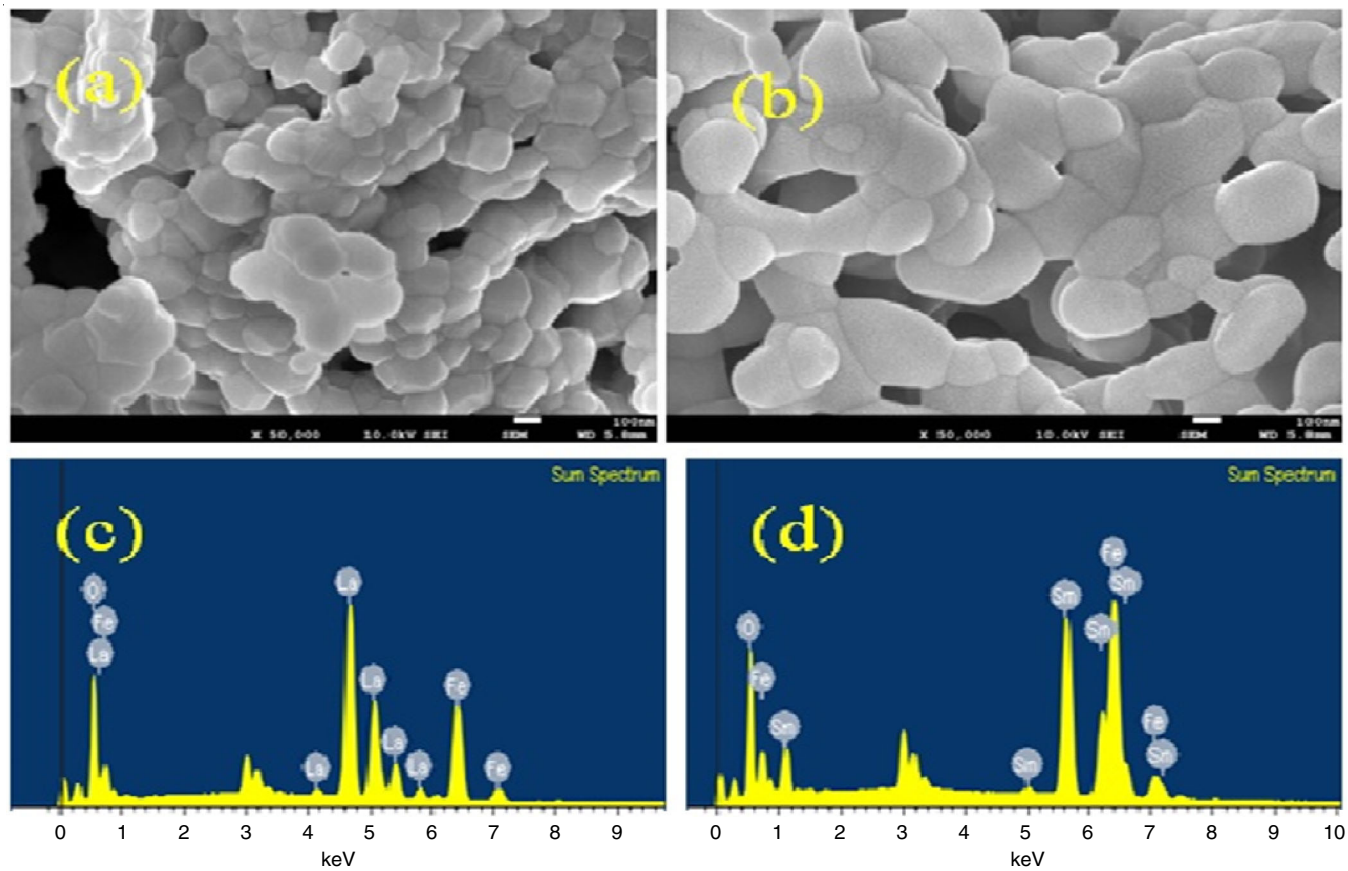

Fig. 5. (a,b) FESEM of iron excess of LFO and SFO and (c,d) EDS of iron excess of LFO and SFO

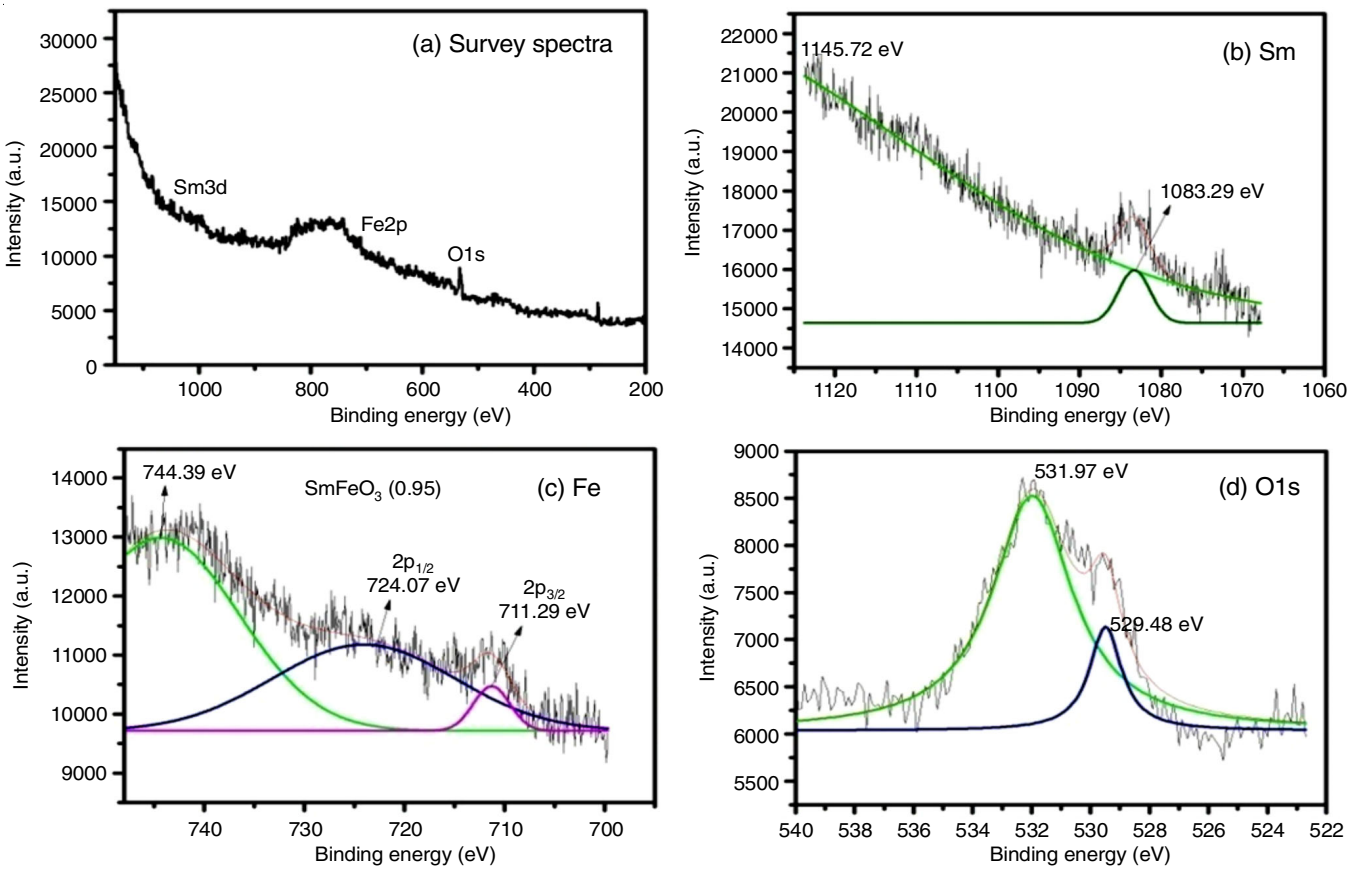

Fig. 6. XPS spectra of iron difficiency of SFO-800 photo catalyst: (a) survey spectra, (b) Sm 3d, (c) Fe 2p and (d) O1s

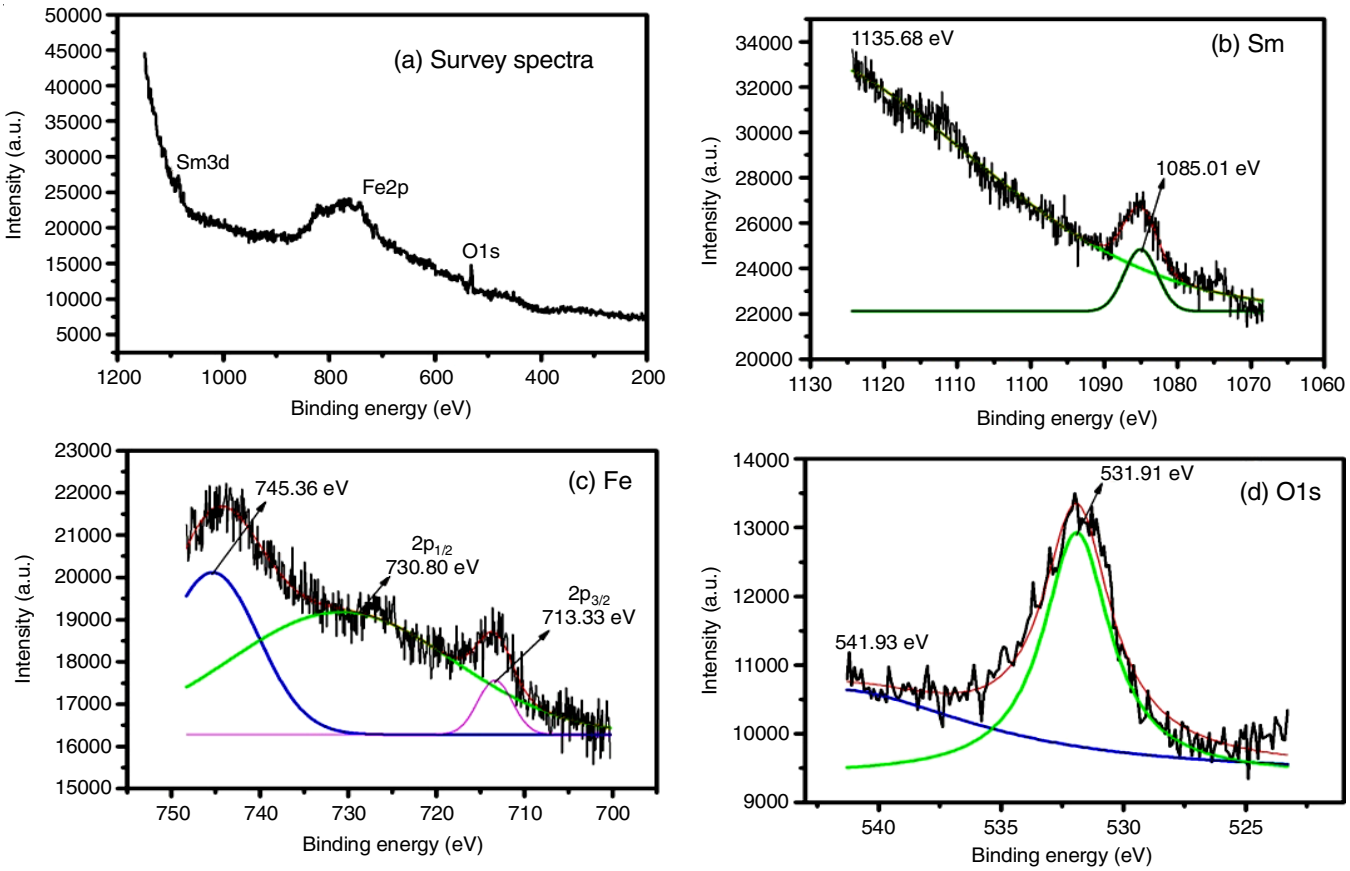

Fig. 7. XPS spectra of iron excess of SFO-800 photo catalyst: (a) survey spectra, (b) Sm3d, (c) Fe2p and (d) O1s

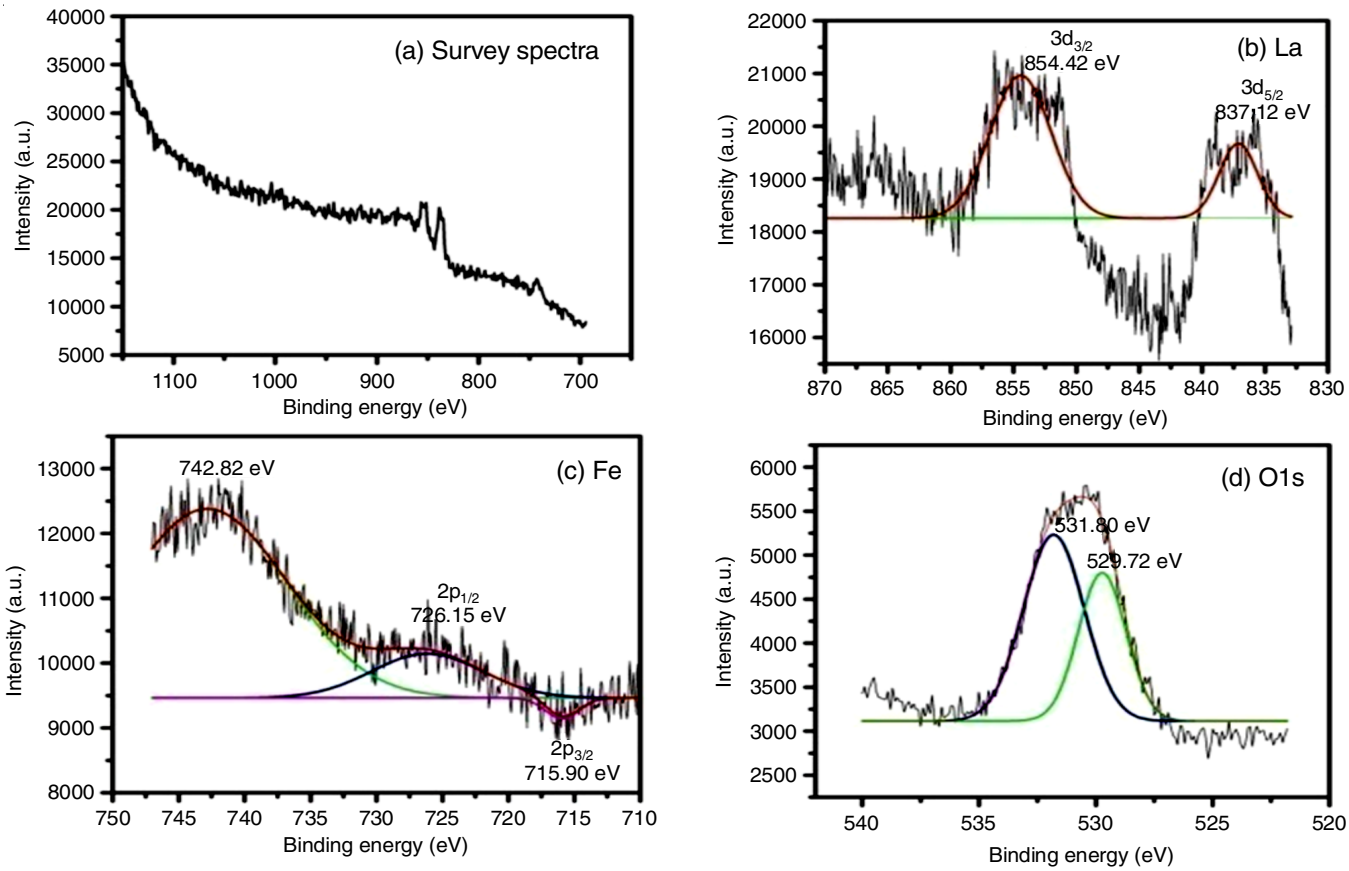

Fig. 8. XPS spectra of iron deficiency of LFO-800 photo catalyst: (a) survey spectra, (b) La3d, (c) Fe 2p and (d) O1s

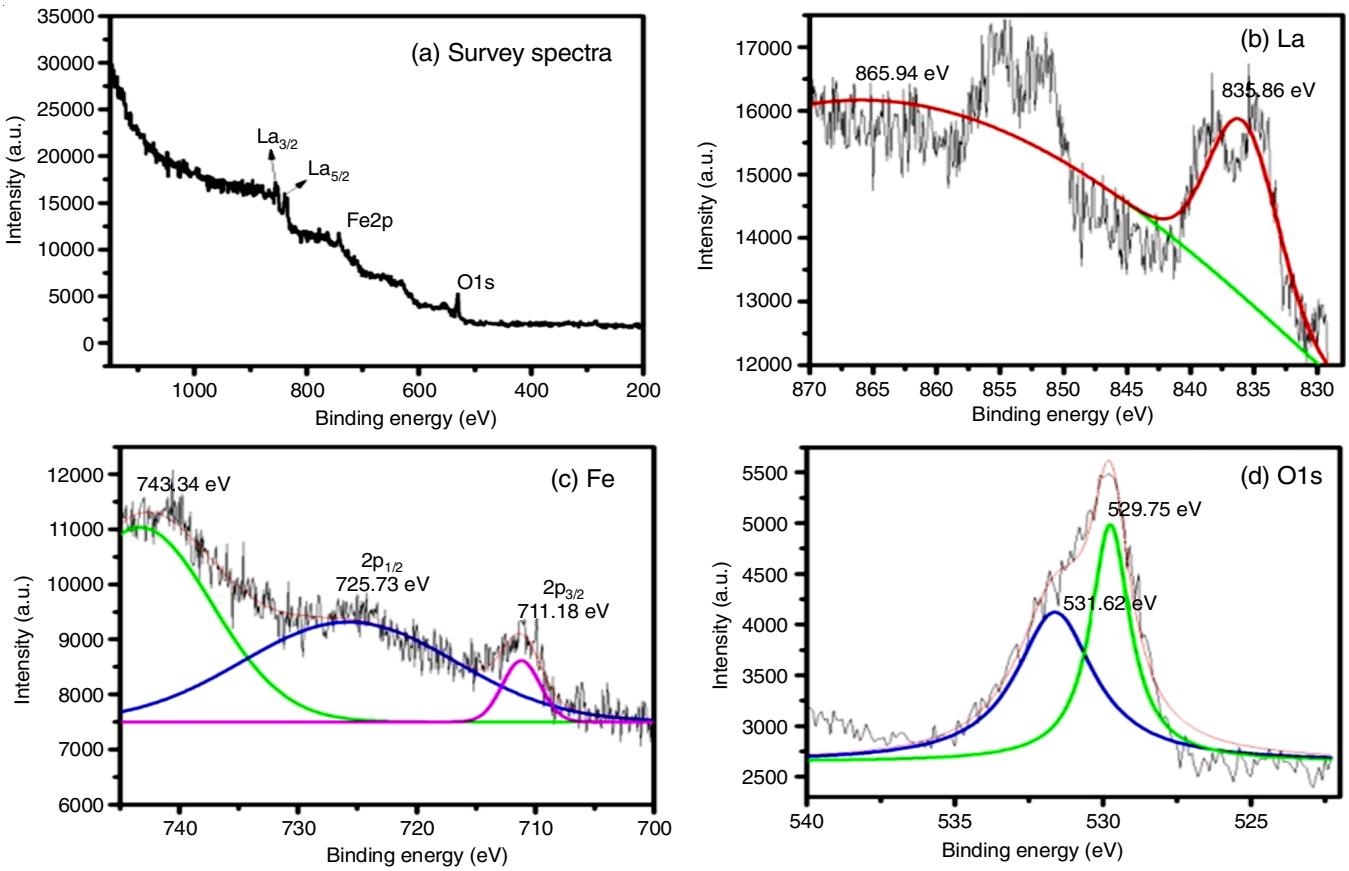

Fig. 9. XPS spectra of iron excess of LFO-800 photo catalyst: (a) survey spectra, (b) La3d, (c) Fe 2p and (d) O1s

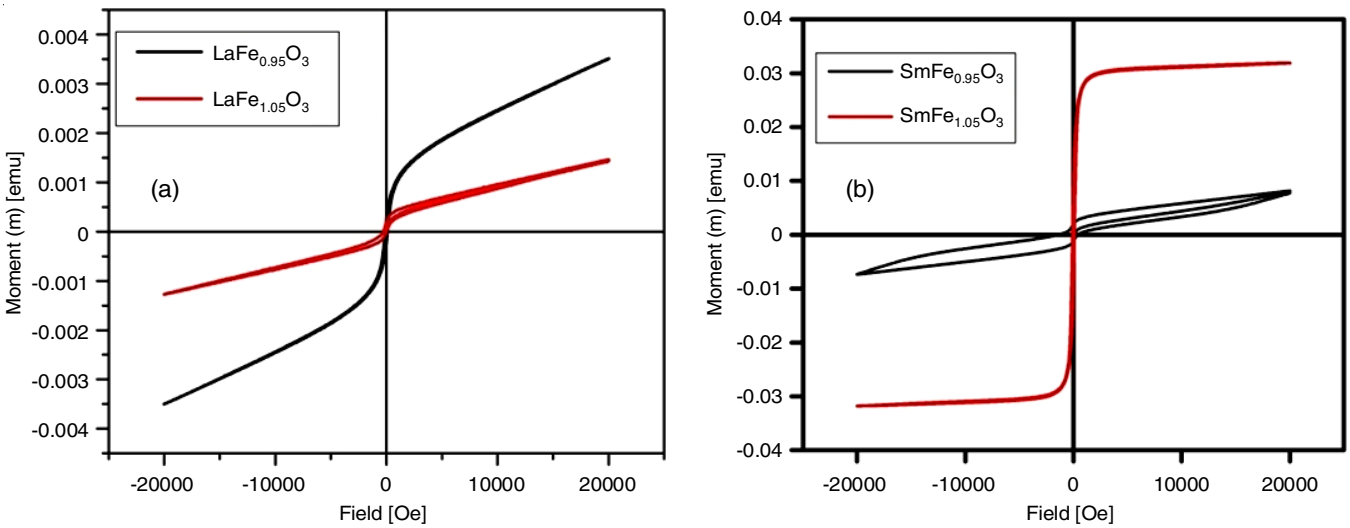

Fig. 10. VSM analysis of excess and deficiency of iron in LFO (a) and SFO (b) perovskite materials

binding energies in comparison to the usual peak values [27] compared to normal peak values following La-Fe interactions, fitted binding energies had lower and higher binding energies. The oxygen (O^{2-}) in the $LaFeO_3$ perovskite lattice was identified in Fig. 8d and 9d by two peaks at 530.30 eV and 532.10 eV.

VSM analysis: At 25 ºC, a vibrating sample magnetometer (VSM) was used to record magnetization (M) and field (H) hysteresis loops. Bulk magnetization and mild ferromagnetism may arise from the statistical distribution of Fe^{3+} inside the octahedral structure, along with the emergence of lattice defects, which can lead to bulk magnetization and weak ferromagnetic characteristics [28,29].

In this work, the room temperature magnetization obtained with varying magnetic fields 20 kOe for synthesized perovskites are shown in Fig. 10. Among the four studied samples, LFO (with iron deficiency) exhibits paramagnetic behaviour and higher saturation magnetization (M), as shown in Fig. 10a. On the other hand, SFO (with excess iron) also displays paramagnetic nature, as depicted in Fig. 10b. Both of these perovskites are capable of absorbing more visible light during the photodegradation process, acting effectively as photocatalysts. The remaining two samples, however, exhibit weak ferromagnetic behaviour, as reported earlier [30].

Conclusion

This study provides insights into the influence of iron stoichiometry on the magnetic and structural properties of $SmFeO_3$ (SFO) and $LaFeO_3$ (LFO) perovskites, synthesized *via* an efficient sol-gel method. The orthorhombic structure and phase purity, irregular morphology of above compounds conformed by powder XRD and FESEM analysis. Further the elemental composition and the surface architecture and chemical valence state of key elements of above perovskites by EDS and XPS analysis. The VSM analysis revealed that iron-deficient $LaFe_{0.95}O_3$ exhibited paramagnetic behaviour with higher saturation magnetization (MS), while iron-excess $SmFe_{1.05}O_3$ also displayed paramagnetic behaviour. Further investigations into the influence of iron stoichiometry on other functional properties, such as electrical conductivity or catalytic activity, could broaden the scope of these findings.

ACKNOWLEDGEMENTS

The authors thank Director, Central Facilities for Research & Development (CFRD) and Department of Chemistry, Osmania University for providing the essential research infrastructures.

CONFLICT OF INTEREST

The authors declare that there is no conflict of interests regarding the publication of this article.

REFERENCES

1. W. Li, Z.-M. Wang, F. Deschler, S. Gao, R.H. Friend and A.K. Cheetham, *Nat. Rev. Mater.*, **2**, 16099 (2017); https://doi.org/10.1038/natrevmats.2016.99
2. N.J. Jeon, J.H. Noh, Y.C. Kim, W.S. Yang, S. Ryu and S.I. Seok, *Nat. Mater.*, **13**, 897 (2014); https://doi.org/10.1038/nmat4014
3. J.A. Dias, M.A.S. Andrade Jr., H.L.S. Santos, M.R. Morelli and L.H. Mascaro, *ChemElectroChem*, **7**, 3173 (2020); https://doi.org/10.1002/celc.202000451
4. S. Heo, G. Seo, Y. Lee, D. Lee, M. Seol, J. Lee, J.B. Park, K. Kim, D.J. Yun, Y.S. Kim, J.K. Shin, T.K. Ahn and M.K. Nazeeruddin, *Energy Environ. Sci.*, **10**, 1128 (2017); https://doi.org/10.1039/C7EE00303J
5. M. Saliba, T. Matsui, K. Domanski, J.-Y. Seo, A. Ummadisingu, S.M. Zakeeruddin, J.-P. Correa-Baena, W.R. Tress, A. Abate, A. Hagfeldt and M. Grätzel, *Science*, **354**, 206 (2016); https://doi.org/10.1126/science.aah5557
6. E.A. Alharbi, A.Y. Alyamani, D.J. Kubicki, A.R. Uhl, B.J. Walder, A.Q. Alanazi, J. Luo, A. Burgos-Caminal, A. Albadri, H. Albrithen, M.H. Alotaibi, J.E. Moser, S.M. Zakeeruddin, F. Giordano, L. Emsley and M. Gratzel, *Nat. Commun.*, **10**, 3008 (2019); https://doi.org/10.1038/s41467-019-10985-5
7. N. Ahn, D.Y. Son, I.H. Jang, S.M. Kang, M. Choi and N.-G. Park, *J. Am. Chem. Soc.*, **137**, 8696 (2015); https://doi.org/10.1021/jacs.5b04930
8. L. Zhang, L. Mei, K. Wang, Y. Lv, S. Zhang, Y. Lian, X. Liu, Z. Ma, G. Xiao, Q. Liu, S. Zhai, S.i Zhang, G. Liu, L. Yuan, B. Guo, Z. Chen, K. Wei, A. Liu, S. Yue, G. Niu, X. Pan, J. Sun, Y. Hua, W.-Q. Wu, D. Di, B. Zhao, J. Tian, Z. Wang, Y. Yang, L. Chu, M. Yuan, H. Zeng, H.-L. Yip, K. Yan, W. Xu, L. Zhu, W. Zhang, G. Xing, F. Gao and L. Ding, *Nano-Micro Lett.*, **15**, 177 (2023); https://doi.org/10.1007/s40820-023-01140-3

9. P. Huang, Q. Chen, K. Zhang, L. Yuan, Y. Zhou, B. Song and Y. Li, *J. Mater. Chem. A Mater. Energy Sustain*., **7**, 6213 (2019); https://doi.org/10.1039/C8TA11841H
10. B.W. Park, B. Philippe, S.M. Jain, X. Zhang, T. Edvinsson, H. Rensmo, B. Zietz and G.J. Boschloo, *J. Mater. Chem. A Mater. Energy Sustain*., **3**, 21760 (2015); https://doi.org/10.1039/C5TA05470B
11. X. Liu, Y. Wang, F. Xie, X. Yang and L. Han, *ACS Energy Lett.*, **3**, 1116 (2018); https://doi.org/10.1021/acsenergylett.8b00383
12. A. Guerrero, J. You, C. Aranda, Y.S. Kang, G. Garcia-Belmonte, H. Zhou, J. Bisquert and Y. Yang, *ACS Nano*, **10**, 218 (2016); https://doi.org/10.1021/acsnano.5b03687
13. D. Shi, V. Adinolfi, R. Comin, M. Yuan, E. Alarousu, A. Buin, Y. Chen, S. Hoogland, A. Rothenberger, K. Katsiev, Y. Losovyj, X. Zhang, P.A. Dowben, O.F. Mohammed, E.H. Sargent and O.M. Bakr, *Science*, **347**, 519 (2015); https://doi.org/10.1126/science.aaa2725
14. N. Aristidou, C. Eames, I. Sanchez-Molina, X. Bu, J. Kosco, M.S. Islam and S.A. Haque, *Nat. Commun*., **8**, 15218 (2017); https://doi.org/10.1038/ncomms15218
15. J. Zhao, Y. Deng, H. Wei, X. Zheng, Z. Yu, Y. Shao, J.E. Shield and Huang, *Sci. Adv.*, **3**, eaao5616 (2017); https://doi.org/10.1126/sciadv.aao5616
16. J.H. Noh, S.H. Im, J.H. Heo, T.N. Mandal and S.I. Seok, *Nano Lett*., **13**, 1764 (2013); https://doi.org/10.1021/nl400349b
17. W.S. Yang, B.W. Park, E.H. Jung, N.J. Jeon, Y.C. Kim, D.U. Lee, S.S. Shin, J. Seo, E.K. Kim and J.H. Noh, *Science*, **356**, 1376 (2017); https://doi.org/10.1126/science.aan2301
18. R. Prasanna, A. Gold-Parker, T. Leijtens, B. Conings, A. Babayigit, H.G. Boyen, M.F. Toney and M.D. McGehee, *J. Am. Chem. Soc*., **139**, 11117 (2017); https://doi.org/10.1021/jacs.7b04981
19. G.A.H. Mekhemer, H.A.A. Mohamed, A. Bumajdad and M.I. Zaki, *Sci. Rep.*, **13**, 7453 (2023); https://doi.org/10.1038/s41598-023-34065-3
20. S.B. Hammouda, F. Zhao, Z. Safaei, D.L. Ramasamy, B. Doshi and M. Sillanpää, *Appl. Catal. B*, **233**, 99 (2018); https://doi.org/10.1016/j.apcatb.2018.03.088
21. G. Balraj, K. Rammohan, A. Anilkumar and D. Ayodhya, *Res. J. Chem. Environ*., **5**, 36 (2023).
22. H. Chang, E. Bjørgum, O. Mihai, J. Yang, H.L. Lein, T. Grande, S. Raaen, Y.-A. Zhu, A. Holmen and D. Chen, *ACS Catal*., **10**, 3707 (2020); https://doi.org/10.1021/acscatal.9b05154
23. R. Zhang, N. Dubouis, M. Ben Osman, W. Yin, M.T. Sougrati, D.A.D. Corte, D. Giaume and A. Grimaud, *Angew. Chem*., **131**, 4619 (2019); https://doi.org/10.1002/ange.201814075
24. J. Kojcinovic, M. Sahu, S. Hajra, D. Tatar, T. Klaser, Z. Skoko, Z. Jaglicic, E. Sadrollahi, F.J. Litterst, H.J. Kim and I. Djerdj, *Mater. Chem. Front*., **6**, 1116 (2022); https://doi.org/10.1039/D1QM01565F
25. E.K. Abdel-Khalek, M.A. Motawea, M.A. Aboelnasr and H.H. El-Bahnasawy, *Physica B*, **624**, 413415 (2022); https://doi.org/10.1016/j.physb.2021.413415
26. J. Dai, Y. Zhu, Y. Zhong, J. Miao, B. Lin, W. Zhou and Z. Shao, *Adv. Mater. Interfaces*, **6**, 1801317 (2019); https://doi.org/10.1002/admi.201801317
27. B. Han, A. Grimaud, L. Giordano, W.T. Hong, O. Diaz-Morales, L. Yueh-Lin, J. Hwang, N. Charles, K.A. Stoerzinger, W. Yang, M.T.M. Koper and Y. Shao-Horn, *J. Phys. Chem. C*, **122**, 8445 (2018); https://doi.org/10.1021/acs.jpcc.8b01397
28. B.-J. Kim, E. Fabbri, D.F. Abbott, X. Cheng, A.H. Clark, M. Nachtegaal, M. Borlaf, I.E. Castelli, T. Graule and T.J. Schmidt, *J. Am. Chem. Soc*., **141**, 5231 (2019); https://doi.org/10.1021/jacs.8b12101
29. A. Nenning, A.K. Opitz, C. Rameshan, R. Rameshan, R. Blume, M. Hävecker, A. Knop-Gericke, G. Rupprechter, B. Klötzer and J. Fleig, *J. Phys. Chem. C*, **120**, 1461 (2016); https://doi.org/10.1021/acs.jpcc.5b08596
30. S. Chandel, P. Thakur, S.S. Thakur, A. Sharma, J.-H. Hsu, M. Tomar, V. Gupta and A. Thakur, *Mater. Chem. Phys.*, **204**, 207 (2018); https://doi.org/10.1016/j.matchemphys.2017.10.042